Mass Transfer Advantage of Hierarchical Structured Cobalt-based Catalyst Pellet for Fischer-Tropsch Synthesis

congcong Niu[1], Hansheng Li[2], Ming Xia[1], Jungang Wang[1], Congbiao Chen[1], Zhongyi Ma[1], Litao Jia[1], Bo Hou[1], and Debao Li[1]

[1]Chinese Academy of Sciences Institute of Coal Chemistry
[2]State Key Laboratory of Fluorinated Functional Membrane Materials

September 14, 2020

Abstract

The low effectiveness factor of catalyst pellet caused by high internal diffusion limitation is a common issue in fixed-bed reactor. Nevertheless, hierarchical structured catalyst provides a promising solution for the contradiction between reaction activity and diffusion efficiency in large catalyst pellets. Herein, we studied the effect of pore structure parameters of the meso-macroporous catalyst on Fischer-Tropsch synthesis performances through experiment and pellet scale reaction-diffusion simulation. The pellet simulation firstly elucidated the reason for the significant improvement on activity and product selectivity for the meso-macroporous catalyst observed in our experiment. Further optimization via pellet simulation indicated the critical influences of wax filling degree and that the perfect matching between reaction and mass transfer rates by increasing macropore size and adjusting porosity within pellet enables the C5+ space-time yield to the maximum. This work could provide a theoretical guideline for the engineering design of the hierarchical structured catalyst pellet.

KEYWORDS

Fischer-Tropsch synthesis, Pellet simulation, Hierarchical structure, Internal diffusion limitation, Mass transfer enhancement

INTRODUCTION

Fischer-Tropsch synthesis (FTS), playing an essential role in the production of liquid fuels and/or chemicals from non-petroleum fossil fuels (coal, natural gas, biomass etc.), has drawn great attention due to the environmental and political considerations, the changes in world fossil energy reserves and the improvements to the FTS technology[1-3] .

Fixed-bed reactors have been widely adopted in low-temperature cobalt-based FTS process, because of the easy separation of catalysts from heavy waxy products, easy to scale-up, low maintenance and low losses due to attrition [2]. Although the fixed-bed FTS technology has been commercially applied worldwide, the trade-off between diffusion length in one single pellet and the pressure drop on the bed length is still a substantial issue for current fixed-bed reactor study [4]. For instance, fixed-bed reactors generally require large catalyst pellets (1-3 mm) to ensure proper pressure drop at specific capacity per reactor [5], while such millimeter-scale catalyst pellets are proved to suffer from severe internal diffusion limitation and the resulting inefficient utilization of active cobalt species and excessive methane formation[5-9]. Therefore, a great number of studies have been devoted to developing a viable catalyst that can balance high product yield and reasonable pressure drop simultaneously.

How to effectively enhance intraparticle mass transfer is the kernel to engineering FTS catalyst pellet and achieving this balance. According to the definition of Thiele modulus $\Phi = L(k\rho_s/D_e)^{1/2}$[10], decreasing

characteristic diffusion distance (L) could help alleviate the mass transfer restrictions in catalyst pellet. The eggshell catalyst with active species only deposited in the outer portion of the pellet while keeping the size of the pellet unchanged is an attractive solution to shorten the diffusion length independently. The eggshell catalysts have been applied in FTS through both experimental [6,11,12] and modeling studies[5-7]. However, the egg-shell structured pellet could commonly possess a low inventory of active phase and thereby a decrease in volumetric yield [13]. The other approach is to alter the geometry of pellets for reducing the pressure drop of catalyst bed and enhancing the transport process. The simulation studies[4,5,8,14] indicated that in comparison to spherical pellets, more complex shapes, i.e., trilobes or hollow cylindrical pellets, exhibit excellent hydrodynamic, transport characteristics under industrial conditions, whereas, the low mechanical strength for hollow cylinder pellet would limit its industrial application[5].

The approaches mentioned above, either the nonuniform distribution of active components or the adjustment on the geometry of pellets, mainly focus on how to shorten the diffusion distance. Besides, designing the pore spatial structure (bimodal pore or fractal-like structures) is also a practical approach to enhance mass transfer by increasing the effective diffusivity. In catalysis, the hierarchical structured catalyst pellet could simultaneously meet the need of high internal surface for active phase distribution and high mass transfer efficiency[15,16]. Coppens and his coworkers[15,17-21] widely studied the general features of the reaction-diffusion process in spatially distributed pore structure catalyst by simulation. In recent years, the hierarchical pore structured catalysts have been extensively applied in adsorption[22,23] and catalysis processes [24-30]. However, contrary to plenty of reports in FTS focusing on the novel preparation methods of the hierarchical structure and the structure-activity relationships [31-37], little attention has been devoted to the detailed reaction-diffusion process in a hierarchical structured catalyst pellet. Xu et al.[38] prepared a bimodal catalyst and elucidated the reaction-diffusion process inside the pellet using a numerical simulation. Nevertheless, the elaborate investigation on the relationship between pore structure parameters and performances has not been reported in literatures.

In comparison to experimental studies, which can only offer discrete experimental points and trends, the numerical modeling study provides the continuous variation of the apparent reaction performances with structural parameters efficiently and conveniently. At present, steady state continuum pellet models have been widely used to simulate the FTS pellet via coupling reaction and transfer processes[4,5,7,8,14,39,40]. Still, such simulation studies were basically limited to the optimization of the shape or dimension of the FTS catalyst pellet based on the assumption of wax fully filled pellet.

In our previous study by Li [32], one kind of hierarchical structured Co/SiO_2 catalyst with the macropore size of 1074 nm and mesopore size of 4 and 36 nm was prepared and compared with a catalyst having only mesopores. The results proved the effectiveness of hierarchical structure on improving mass transfer. However, the question why the hierarchical structure enhances mass transfer of FTS and how the pore structure parameters quantitatively influence the catalysis performances remains mysterious, which hinders the rational design of FTS catalyst engineering pellet.

Hence, in this work, on one hand, a series of meso-macroporous catalyst pellets (10-20 mesh) with the equivalent mesopore size but various macropore size were synthesized and evaluated for a detailed relationship between macropore size and FTS performances. On the other hand, a 1-dimension steady state continuum model was established to simulate the meso-macroporous catalysts. The simulation results of the pellet with the size of 10-20 mesh reasonably explained the enhancement on mass transfer with increasing macropore size observed in experiments. In addition, the simulation results of the 2 mm pellet give more insights into the effects of pore structure parameters on FTS performances at different operation conditions. A Langmuir-Hinshelwood type kinetics for cobalt-based FTS by Yates and Satterfield[41] corrected by our experiment data and a chain growth probability model [42] were combined to calculate the C_{5+} space-time yield which was used as an index to evaluate the FTS performances. The experimental and simulated results regarding to the intraparticle mass transfer enhancement could provide useful guidance for rational design of industrial FTS catalyst engineering pellet.

2. EXPERIMENTAL

2.1 Catalyst preparation

The meso-macroporous SiO_2 monoliths were prepared by a sol-gel method similar with our previous studies[31,32]. By controlling the rates of phase separation and sol-gel process, the interconnected macropores with various diameter were obtained, while the mesopores were from ammonia etching. The prepared meso-macroporous monoliths were ground into 10-20 mesh as supports and labeled as S0, S50, S150, S280, S440, S1100, S2100 and S6000 respectively according to the diameter of the macropores. A series of cobalt catalysts with the same nominal cobalt loading (15 wt %) were prepared by incipient impregnation method. The obtained supports were impregnated with cobalt nitrate and calcined at 400°C for 6 h after drying at 60°C for 2 h and at 120°C for 4 h successively. The obtained catalysts were labeled as Co/S0, Co/S50, Co/S150, Co/S280, Co/S440, Co/S1100, Co/S2100 and Co/S6000 respectively.

2.2 Catalyst characterization

The textural properties of the samples were obtained combining the N_2 adsorption-desorption isotherms measured by an ASAP-2000 Micromeritics instrument and mercury intrusion isotherms measured using a MicroActive AutoPore Iv 9510 analyzer.

The morphological analysis of the obtained silica monoliths and the prepared catalysts were performed using a JSM-7001F scanning electron microscope (SEM) operated at 5.0-15.0 kV and using a JEM-2010F microscope operated at 200 kV respectively.

X-ray diffraction (XRD) characterization was carried out on a PANalytical Empyrean X'pert powder diffractometer operated at 50 kV and 50 mA with Cu Kα radiation.

H_2 temperature-programmed reduction (H_2-TPR) was performed to obtain reduction profiles of the prepared catalysts using a Zeton Altamira AMI-200 unit. The detailed sample pretreatment, data processing and operation method are the same with our previous report [32].

2.3 Catalyst testing

0.5g of the prepared catalyst (10-20 mesh) diluted with an equal volume of quartz sand, was evaluated in a lab-scale fixed-bed stainless steel reactor (Φ10×500 mm). The other detailed setup used for FTS experiments, including methods and tools, was described in our previous literature[32].

3. MODELING

The model catalyst pellet is assumed as an isothermal and isobaric sphere for common simplicity, and a 1-dimensional steady state continuum model can be used to describe the reaction-diffusion process in the pellet.

The hierarchical pore structure prepared can be simplified as Figure 1 based on the preparation method of the meso-macroporous SiO_2 monoliths in section 2.1. At typical industrial conditions of cobalt-based FTS, the hydrocarbons products (especially waxes) could condense and accumulate in pores and form a thin liquid layer on the external surface of the pellet. Therefore, the syngas must solubilize in the liquid film first and further diffuse into the pores and reach the internal active sites, accompanying with FTS reaction[5,7-9,14,38,42-44]. The external diffusion limitations in the gas and liquid films were assumed to be negligible because of the high gas linear velocity employed in industrial reactors[45]. Since the mesopores formed by ammonia solution etching were mainly dispersed on the internal surface of the macropores and diffusion length in mesopores was relatively short, the internal diffusion limitations in such mesopores was not considered in the pellet modeling.

The following Eq.(1) was adopted to describe the overall stoichiometry of FTS on cobalt catalyst, according to the assumption by Mandic[5] to the average molecular weight of hydrocarbon products for their kinetics experiments with 0.48%Re-25%Co/Al_2O_3 catalyst.

$$CO + \left(\tfrac{13}{6}\right) H_2 = H_2O + (\tfrac{1}{6})C_6H_{14} \quad (1)$$

Fick's law has been widely used in describing the internal transport process in FTS catalyst pellet [5,8,14,45]. For an isothermal spherical pellet, the generalized reaction–diffusion continuity equation at steady state can be expressed as:

$\frac{1}{x^2} \bullet \frac{d}{\mathrm{dx}} \left(x^2 \bullet \frac{d\Psi_i}{\mathrm{dx}}\right) + \upsilon_i \cdot (\phi_i^{'})^2 \cdot \overline{R}_{\mathrm{CO}} = 0 (2)$

The boundary conditions are given as:

$x = 0 : \ \frac{d\Psi_i}{\mathrm{dx}} = 0 \ (3)$

$x = 1 : \Psi_i = \ \frac{c_i^s}{c_{\mathrm{CO}}^s} \ (4)$

Herein, x is the dimensionless distance to the center of the pellet, $x = \frac{r}{r_p}$.$\Psi_i = \ \frac{c_i}{c_{\mathrm{CO}}^s}$ represents the local dimensionless concentration of component i (i = CO, H_2, H_2O and C_6H_{14}).$\overline{R}_{\mathrm{CO}} = \ \frac{R_{\mathrm{CO}}}{R_{\mathrm{CO}}^s}$is the dimensionless reaction rate of CO. υ_i is the stoichiometric coefficient, and equals -1, -13/6, 1 and 1/6 respectively for CO, H_2, H_2O and C_6H_{14}. The dimensionless group$\phi_i^{'} = r_p(\frac{\rho_P(-R_{\mathrm{CO}}^s)}{(D_{e,i} \cdot C_{\mathrm{CO}}^S)})^{1/2}$is comprised of the radius of the pellet, r_p, the pellet density,ρ_p, CO consumption rate at the external surface of the pellet,R_{CO}^s, the effective diffusion coefficient of component$i$, $D_{e,i}$, and CO concentration at the external surface,C_{CO}^S.

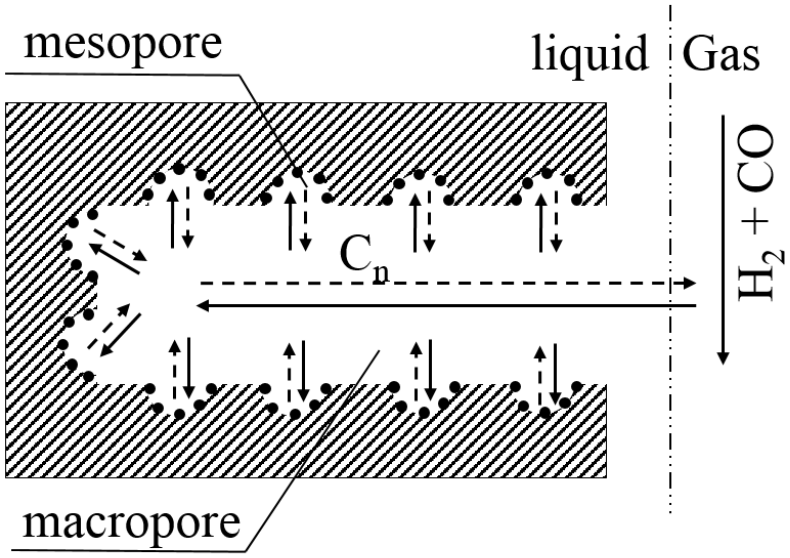

Figure 1. Illustrations of the meso-macropore networks.

3.1 kinetics and chain growth factor model

CO consumption rate with Langmuir-Hinshelwood kinetics by Yates and Satterfield [41] was used in this study. The values of reaction rate constant (k) and adsorption equilibrium constant (a) listed in Table 1S (see Supporting Information) are from the regression of experimental data with 0.48%Re-25%Co/Al_2O_3 catalyst by Mandic et al. [5]. The correction factor (f) in Eq.(5) was used to correct reaction activity based on our experimental data in the absence of diffusion resistance.

$(-R_{\mathrm{CO}}) = \frac{\mathrm{f\ k}\ P_{\mathrm{CO}} P_{H_2}}{(1+a\ P_{\mathrm{CO}})^2} (5)$

A chain growth factor model related to temperature and concentration ratio of H_2 and CO reported by Vervloet,[42] was adopted to calculate the product selectivity within the pellet.

$$\alpha = \frac{1}{1+k_\alpha(\frac{c_{H_2}}{c_{CO}})^\beta exp(\frac{E_\alpha}{R}(\frac{1}{493.15}-\frac{1}{T}))} (6)$$

3.2 Physical properties

The concentrations of species CO, H_2, H_2O and C_6H_{14} dissolved in the wax phase assumed to be in equilibrium with those in the gas phase can be described by Henry's law [5,8,45]. Henry's law constants for gases and light hydrocarbons in n-paraffins were calculated from Marano and Holder's correlation [46].

Wax accumulation in FTS catalyst pores is a non-negligible factor leading to strong internal diffusion limitations because of the low diffusivity of reactants and products in liquid wax[7,43,44]. Considering the huge diffusivity difference in liquid phase and gas phase, the diffusivity in pellet is closely related to the wax filling degree in pores. In the case of pores with wax fully filled, the liquid phase molecular diffusion dominates the mass transfer restrictions while Knudsen diffusion limitations could be neglected. The diffusivity in liquid wax, $D_{i,liq}$, thought to be related to the composition of wax and temperature, can be estimated from Akgerman's correlation [47,48]. Although the assumption of the pellet with wax fully filled has been applied for simplicity in almost all numerical modeling studies of FTS catalyst pellet[5,7-9,14,38,42-44]. The studies by Jess et al.[43,44,49] indicated there might exist only partly filled state in pores under practical industrial FTS conditions. Furthermore, the introduction of macropores in pore structure is in favor of a reduction in the filling degree of liquid wax. Despite this, accurate calculation or measurement of filling degree F at a certain condition is still a complicated and tough task, because of the complex interactions among catalyst apparent reactivity, diffusivity in pores, product distribution, and liquid phase accumulation rate in pores. Since the focus of this study is to compare the performances at various porosity and macropore size, F is assumed as constant with series of values (0.6, 0.7, 0.8, 0.9, 1.0) for simplicity in the following. In the case of the pellet pores with wax partially-filled (F <1), both Knudsen and molecular diffusion contribute to the mass transfer process in the pores, and Eq. (10) proposed by Jess[50] based on the random pore model [51]can be used to calculate the effective diffusivity in the whole pellet scale.

$$D_{eff,i} = (1-F)^2\varepsilon^2 D_{i,g} + \frac{F^2\varepsilon^2(1+3(1-F)\varepsilon)}{1-(1-F)\varepsilon} D_{i,liq} (7)$$

Herein, e is the porosity of the catalyst pellet.$D_{i,g}$, the gas phase diffusivity in pores, can be described by the Wilke-Bosanquet model [45]:

$$\frac{1}{D_{i,g}} = \frac{1}{D_{i,m}} + \frac{1}{D_{i,k}} \ (8)$$

$D_{i,m}$, the molecular diffusivity of component$i$ in the gas mixture of reactants and products in the pore, can be calculated from the binary gas diffusivity$D_{i,j}$ and the molar contenty_i [50].

$$D_{i,m} = \frac{1-y_i}{\sum_{j=1,i\neq j}^{n}(y_i/D_{i,j})} (9)$$

The binary gas diffusivity $D_{i,j}$ can be calculated by the Fuller Method[52] with the temperature T, pressure P, molecular weight of each components M_i, and diffusion volume Σ_v. The value of Σ_v for components used in the present study can be obtained from the literature[52].

$$D_{i,j} = \frac{0.00143T^{1.75}}{PM_{i,j}^{\frac{1}{2}}[(\Sigma_v)_A^{\frac{1}{3}}+(\Sigma_v)_B^{\frac{1}{3}}]^2} (10)$$

$$M_{i,j} = 2\left(\frac{1}{M_i}+\frac{1}{M_j}\right)^{-1} (11)$$

The Knudsen diffusivity $D_{i,k}$ can be calculated based on the kinetic theory of gases [52] with the radius of pore R_p, temperature T and molecular weight M_i.

$$D_{i,k} = 97R_P(\frac{T}{M_i})^{\frac{1}{2}} \ (12)$$

Parameters used in simulation of the 2 mm pellet were listed in Table 1.

Table 1 Parameters for 2 mm pellet simulations

Parameter	Symbol	Unit	Value
Temperature	T	K	473, 493, 513
Total pressure	P	MPa	1.0, 2.0, 3.0, 4.0
H_2/CO	/	/	2.0
Pellet radius	r_p	mm	1.0
Density of support skeleton	ρ_s	kg/m^3	2150
Porosity of the pellet	e	/	0.4-0.85
Mesopore diameter	$d_{p,meso}$	nm	8
Macropore diameter	$d_{p,macro}$	nm	50-800

3.3 Performances parameters

Performances parameters and the calculation equations used in this modeling study were listed in Table 2S (see Supporting Information). Typically, C_{5+} space-time yield ($STY_{C_{5+}}$) in FTS is a key factor, because it is a combination of catalyst apparent activity and selectivity. Therefore, in the following discussion, $STY_{C_{5+}}$ is used as the evaluation criteria for catalyst reaction-diffusion performances.

3.4 Method of solution

The second-order ordinary differential equation, Eq. (5), was first written as two first-order ordinary differential equations, for each component. The obtained system of first-order ordinary differential equations with the boundary conditions specified at two points was then solved by finite different method. The integral terms in performance parameters listed in Table 2S were calculated using trapezoidal rule based on the concentration profiles calculated within the pellet.

4. RESULTS AND DISCUSSION

4.1 Physicochemical Properties

The SEM images of the prepared supports with various macropore size are shown in Figure 2. The sample of S0 exhibited packed aggregates of silica particles (no macropore), while the other samples (S50 ˜ S6000) exhibited a honeycomb structure with macropores. From S50 to S6000, the size of the macropore increased gradually, and the results of SEM observations were in good agreement with those of mercury intrusion porosimetry as shown in Figure 1S(a) (see Supporting Information).

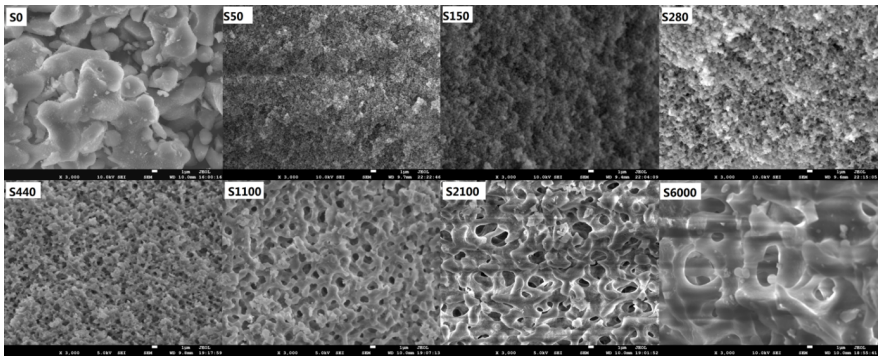

Figure 2 SEM images of the prepared supports.

As shown in Figure 2S (see Supporting Information), the isotherms of the prepared supports and catalysts were of type IV in shape with typical hysteresis loop. The supports of S440, S1100, S2100, S6000 and the corresponding cobalt catalysts(Co/S440, Co/S1100, Co/S2100, Co/S6000) displayed similar type H1 hysteresis loop, which is representative of an adsorbent with a narrow distribution of relatively uniform mesopores[53].

However, for the samples of S50, S150, S280 and the corresponding catalysts, the hysteresis loop shifted to a higher p/p^0, which means the existence of larger pores[34]. Therefore, the nitrogen physisorption should be combined with mercury intrusion porosimetry to obtain the reliable macropore distribution information [53]. The detailed textural properties of the supports and catalysts are listed in Table 2. The large specific surface (˜500 m^2/g), beneficial for active phase dispersion, was mainly attributed to the smaller pores (˜8 nm) produced by ammonia etching. The large pore volume of the supports, beneficial for mass transfer, was due to the presence of macropores. The significant decrease in the specific surface and pore volume of the cobalt-loaded catalysts compared to the supports could be attributed to the partial pore blocking by cobalt crystallites. In summary, except for S0 and Co/S0 which were monodispersed mesopore structure, the other supports and catalyst samples all exhibited meso-macropore structure.

The wide-angle XRD patterns of the prepared catalysts are presented in Figure 1S(b) (see Supporting Information). For all the catalyst samples, peaks appearing in 31.4°, 36.9°, 44.8°, 59.4°, and 65.2° corresponded to the diffractions of Co_3O_4 phase. The average crystallite sizes of Co_3O_4, calculated from the Scherrer equation at the most intense diffraction ($2\vartheta = 36.9°$) are listed in Table 2. Almost all catalysts had similar crystallites size, except Co/S50 and Co/S150 presenting a slightly larger crystallites size, which can be attributed that small macropore diameter of Co/S50 and Co/S150 affects the nucleation and growth of cobalt particle. The typical TEM images of the catalyst samples, as presented in Figure 4S (see Supporting Information), indicated that all catalysts exhibited a worm-hole-like pore structure, which could be attributed to the mesopores of 7.76˜9.60 nm and the active species were uniformly distributed.

Table 2 The physical properties of the catalyst samples.

Samples	A_{BET} (m^2/g)	V_{Meso} [a] (cm^3/g)	d_{Meso} [a] (nm)	d_{Macro} [b] (nm)	$d(Co_3O_4)$	d(Co) [c]	D (%) [d]
S0	408.33	0.80	7.76	\			
S50	517.60	1.42	9.60	50			
S150	526.61	1.23	9.10	150			
S280	535.92	1.12	9.40	280			
S440	503.84	1.08	9.20	440			
S1100	497.54	0.92	8.70	1100			
S2100	496.99	0.85	8.30	2100			
S6000	488.40	0.80	7.80	6000			
Co/S0	300.60	0.55	8.20	0	12.10	9.08	10.58
Co/S50	412.70	1.16	9.60	50	16.20	12.15	7.90
Co/ S150	429.62	1.02	9.10	150	16.50	12.38	7.76
Co/ S280	427.50	0.94	9.40	280	12.10	9.08	10.58
Co/ S440	378.97	0.80	9.20	440	12.50	9.38	10.24
Co/S1100	388.44	0.71	8.40	1100	12.70	9.53	10.08
Co/S2100	378.51	0.63	7.93	2100	12.30	9.23	10.40
Co/S6000	371.10	0.59	7.67	6000	12.70	9.53	10.08

[a]: calculated from N_2adsorption-desorption data [b]: calculated from Hg intrusion data

[c]: $d(Co) = 0.75\ d(Co_3O_4)$ [d]: $D\ (\%) = 96/d(Co)$

All catalysts presented similar reduction behavior according to the reduction profiles of the catalysts studied by H_2-TPR, as seen in Figure 1S(c) (see Supporting Information). The reduction peaks at 200°C-300°C, 250°C-500°C, 550°C-900°C were usually contributed to the reduction of Co_3O_4 to CoO, CoO to metallic Co[31,32,37] and the reduction of amorphous Co/silica phase, individually, Co/S50 and Co/S150 had relatively larger area of the second reduction peak which was mainly caused by the larger crystallites size of these two catalysts. Besides, the quite weak reduction peaks (at 250°C-500°C) of all catalysts indicated a good

reducibility and a weak interaction between active phase and supports.

4.2 Reaction performance assessment over hierarchical catalyst

After 24 h of reaction with the steady state achieved, the performances of the prepared FTS catalysts are collected as in Table 3S (see Supporting Information) and Figure 3. The large catalyst pellets (10-20 mesh) of FTS, commonly recognized to bear severe internal diffusion limitations, were employed to investigate the mass transfer enhancement with the meso-macropore structure.

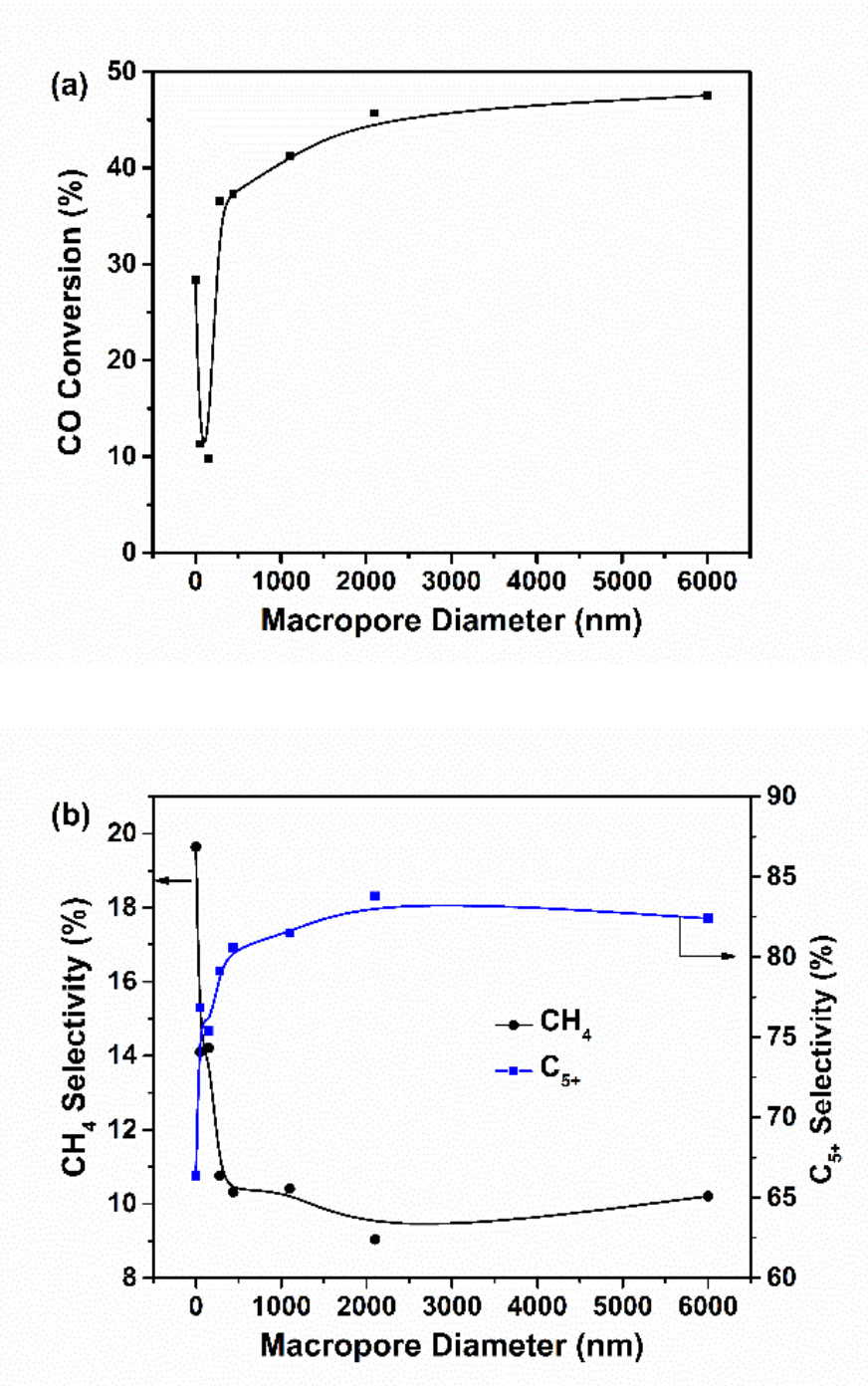

Figure 3 Effect of macropore diameter on (a) CO conversion and (b) CH_4 and C_{5+} selectivities

It can be seen from Figure 3(a), that the diameter of macropores played a positive role in improving reaction activity, except Co/S50 and Co/S150. The relatively lower reaction activity of Co/S50 and Co/S150 could be attributed to the larger cobalt crystallites size and lower dispersion. In general, an obvious increase in CO conversion was observed over the range Co/S0 to Co/S2100, because of the enhancement of diffusivity with the introduction of macropores. However, as the macropore size was larger than 2100 nm, there was only a slight increase in CO conversion with further increasing macropore size, suggesting that the internal diffusion limitation had been nearly ruled out under this condition. The product selectivity results, shown in Figure 3(b), provided more conclusive evidence. For Co/S0 with only mesopore and no macropore, the methane selectivity was up to 19.64 %, while C_{5+} selectivity was only 66.36 %. The poor product selectivity was caused by the severe internal diffusion limitation leading to a higher H_2/CO ratio, which would favor methane formation and chain termination reactions. Obviously, the introduction of macropores was beneficial for improving production selectivity by diminishing the influence of the internal diffusion limitations and further reducing the H_2/CO ratio in pellet. As macropores were larger than 2100 nm, the product selectivity became nearly constant with pore size, which was an indicator of the elimination of internal diffusion limitations. Although the variation trend of FTS activity and selectivity with the macropore size had been investigated by the experiment, the quantitative relationship between FTS performances and pore structure parameters were still needed to gain a deep insight into the diffusion-reaction interplay process.

4.3 Simulation results of catalysts used in experiment

Based on the analysis of the experimental data above, the activity data for macropore size of 6000 nm could be regarded as the intrinsic performance of cobalt-based catalyst prepared in the present study, except Co/S50 and Co/S150 which had larger crystalline size than the others. Therefore, this activity data was used to calculate the correction factor f for the kinetic model used in the pellet model. Through a "lumping" method derived by Liu [54], the CO conversion at the outlet of the bed was calculated and the value of f was obtained to be 1.687.

However, it is almost infeasible to validate the pellet model directly with the experiment data due to the lack of accurate value of filling degree (F) under reaction conditions. Conversely, the established pellet model was applied to fit the value of wax filling degree $F$with the experimental data. The macroporosity was used to calculate the effective diffusivity within pellet, because macropores was the main sources of mass transfer restriction according to the assumption in section 3 and Figure 1. The fitted filling degree, as seen in Table 3 indicated that the pores were wax fully filled for the monodisperse catalyst (with mesopore size of 8 nm) under the reaction conditions, which was consistent with the general claims in literatures[9,43]. The results revealed that introducing macropores was in favor of decreasing wax filling degree, and the filling degree was only 0.2 as the macropore was 6000 nm. However, the filling degree was always larger than 0.9 as the macropore size in the range of 280 to 2100 nm. The high filling degree could be attributed to the low gas velocity in lab-scale fixed-bed reactor, which was unfavorable to the vapor flow out of the pores according to the definition of the mass transfer coefficient β_i [43] :

$$\beta_i = \frac{\mathrm{Sh} \bullet D_i}{L} \quad (13)$$

Here, L is the characteristic length of the catalyst pellet, D_i is the diffusivity of product i in feed/product gas mixture and Sh is the Sherwood number can be calculated by correlating Reynolds number Re and Schmidt number Sc:

$$\mathrm{Sh} = 2 + 0.664\mathrm{Re}^{1.5}\mathrm{Sc}^{0.5} \quad (14)$$

Table 3 Calculation results of filling degree within the catalysts in experiment based on the pellet model [a].

Catalysts	ε_{macro} [b]	CO Conv.(%)	$R_{CO,exp}$ (mol/$kg_{support}$·s)	η_{exp} [c]	η_{cal}	Filling degree (F)
Co/S0	\	28.36	6.351×10^{-3}	0.597	0.596	1.000

Catalysts	ε_{macro} [b]	CO Conv.(%)	$R_{CO,exp}$ (mol/kg$_{support}$·s)	η_{exp} [c]	η_{cal}	Filling degree (F)
Co/S280	0.563	36.53	8.181×10^{-3}	0.768	0.767	0.953
Co/S440	0.574	37.31	8.356×10^{-3}	0.785	0.787	0.953
Co/S1100	0.593	41.20	9.227×10^{-3}	0.867	0.867	0.941
Co/S2100	0.606	45.71	1.024×10^{-2}	0.962	0.961	0.907
Co/S6000	0.444	47.54	1.065×10^{-2}	1.000	0.999	0.200

[a] Reaction conditions: catalyst size of 10-20 mesh (1.34 mm used in simulation), T = 200 °C, P = 2 MPa, H_2/CO = 2, GHSV = 4.8 L/g_{cat}·h.

[b] Macroporosity calculated based mercury intrusion volume from 50 to 30000 nm.

[c] $\eta_{exp} = R_{CO,exp} / R_{CO,exp,(\text{for Co/S6000})}$.

The simulation results also indicated that the increase of macroporosity from 0.563 to 0.606 also contributed to the enhancement of mass transfer with increasing macropore size. However, the increase of Knudsen diffusion coefficient only played a slight effect, because the Knudsen diffusion was not the limiting factor as the macropore size was larger than 200 nm according to the relationship between gas phase diffusivity and pore size. (see Figure 5S in Supporting Information).

4.4 Simulation results of a 2 mm catalyst pellet

Based on our meso-macropore model with the fixed mesopore size of 8 nm, the C_{5+} space-time yield ($STY_{C_{5+}}$) in FTS was optimized by adjusting the porosity and macropore diameter over the range of 50 to 800 nm. The performance of the monodisperse catalyst pellet with the pore size of 8 nm was given as a benchmark for comparison. The simulation results at the temperature of 473, 493and 513 K are displayed in Figure 4.

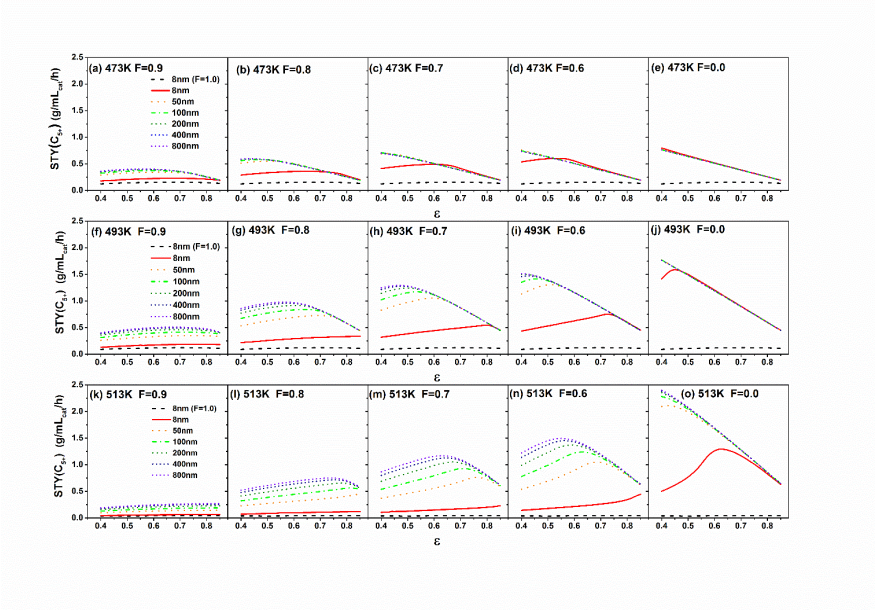

Figure 4 $STY_{C_{5+}}$ of the meso-macropore catalyst pellets with different macropore diameter and filling degree at the temperature of 473, 493 and 513 K. The pressure was 2.0 MPa, H_2/CO was 2.0 and other simulation parameters were adopted from Table 1.

4.4.1 Filling degree

Although the fitted value of wax filling degree in the meso-macroporous catalysts used in the experiment was commonly high and around 0.9, in real industry conditions, the high gas velocity around catalyst pellets would promote the product flow out of the pores. Hence, in the modeling study of a 2 mm industrial pellet, the filling degree range from 1.0 to 0.6 was considered. Figure 4 indicated that the decrease in wax filling degree had a significant positive effect on $STY_{C_{5+}}$, especially in the temperature of 493 and 513 K, no matter on monodisperse or bidisperse structured catalyst pellet. Specifically speaking, the optimal $STY_{C_{5+}}$ over the monodisperse catalyst, with wax fully filled, ranged from 0.156 to 0.042 $g/mL_{cat}{\cdot}h$ with the temperature from 473 to 513 K, which were much lower than that at the partially filled conditions. In contrast, under full gas condition (F =0), the performance curves of meso-macroporous catalyst were nearly coincide in Figures 6(e), 6(j) and 6(o), indicating the elimination of the internal diffusion limitations. Therefore, wax accumulation in catalyst pores was a critical reason for internal diffusion limitation, which was consistent with the general views in the literature [7,43,44]. Considering that the products of low-temperature cobalt-based FTS are mainly long-chain hydrocarbons which are prone to liquefy and condensate in the catalyst pores[3,43], it is necessary to study the approaches to inhibiting wax filling. From the pellet engineering design perspective, a higher surface to volume ratio, the introduction of macropores, higher porosity and properly hydrophilic modification of inner pore surface are all tend to reduce the pore filling degree.

4.4.2 Porosity

It is generally accepted that increasing particle porosity is beneficial for improving diffusion process. However, increasing porosity also decreases particle density and the density of active cobalt sites with constant load capacity per mass catalyst. Therefore, there exists an optimal porosity that attains the highest $STY_{C_{5+}}$, which is the vertex of each curve in Figure 4. For the temperature of 513 K and filling degree of 0.6, connecting the vertices of each curve gets a line, which can be defined as reaction-diffusion boundary line (denoted as boundary line for short, see Figure 5). The rates of reaction and diffusion reach a perfect matching at each point of the line. We defined the lower left side of the boundary line as diffusion-limited region, where apparent reaction rate was controlled by mass transfer, and hence increasing porosity was helpful to improve diffusion efficiency and increase$STY_{C_{5+}}$. Correspondingly, the upper right side was defined as reaction-limited region, where reaction rate was the controlling factor and increasing porosity was disadvantageous to increase $STY_{C_{5+}}$.

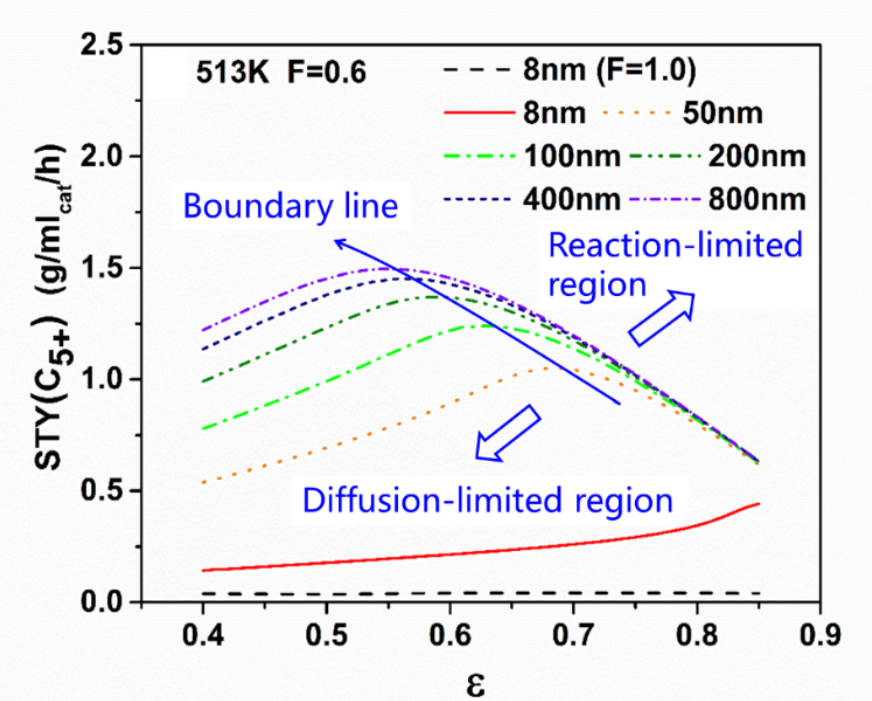

Figure 5 $STY_{C_{5+}}$ of the meso-macropore catalyst pellets with different macropore diameter at 513 K and the filling degree of 0.6. The total pressure was 2.0 MPa, H_2/CO was 2.0 and other simulation parameters were adopted from Table 1.

4.4.3 Macropore diameter

Since molecular diffusivity is independent of pore size, only changing the macropore size barely affect the mass transport process in pores with wax fully filled. Therefore, we only considered the partially-filled conditions to investigate the influences of pore size. The results in Figure 4 revealed that$STY_{C_{5+}}$ was more sensitive to pore size under low filling degree conditions than that under high filling degree conditions, because low filling degree means high gas fraction in pores. Furthermore, in the diffusion-limited region, at the temperature of 493 and 513 K, the increase in macropore size from 50 to 200 nm could significantly improve$STY_{C_{5+}}$, and then $STY_{C_{5+}}$ slightly increased with further increasing the macropore size to 800 nm. This is because the Knudsen diffusivity is in direct proportion to pore size, and the gas phase effective diffusivity could be substantially improved by increasing the pore size below 200 nm (see Figure 5S in Supporting Information). As the pore size was larger than 200 nm, the value of Knudsen diffusivity was far larger than that of molecular diffusivity. In this case, molecular diffusivity became the main controlling factor for the gas phase effective diffusivity. In the reaction-limited region, although the gas phase effective diffusivity can also be improved by increasing macropore size, $STY_{C_{5+}}$ was almost independent on pore size. Accordingly, the macropore diameter of 200 nm was preferred for the meso-macroporous catalyst pellets at the temperature range of 473-513 K.

4.4.4 Optimization under different temperature

The dependence of $STY_{C_{5+}}$ on macropore size was enhanced at higher temperature, because the resulting higher intrinsic reactivity would sharpen the influence of internal diffusion limitation. Therefore, the elimination of mass transfer restriction via elaborate engineering design of the hierarchical structured pellet is extremely essential at high reactivity conditions.

Under the total pressure of 2.0 MPa, the filling degree of 0.6, the H_2/CO mole ratio of 2.0, the reaction

temperature of 473, 493 and 513 K, the optimal porosity for the meso-macroporous catalyst pellet was in the range of 0.40 to 0.59.$STY_{C_{5+}}$ of the catalyst pellet ranged from 0.738 to 1.370 g/mL_{cat}·h with the mesopore and macropore size of 8 nm and 200 nm respectively. And it was 22-210 % higher than that of monodisperse catalyst under the same conditions. Therefore, it is highly advantaged to utilize the hierarchical structured catalyst pellet for FTS.

4.4.5 Optimization under different pressure

Based on the simulation result at the temperature of 513 K, the pressure of 2.0 MPa, filling factor of 0.6, the simulations under different pressure (1.0, 3.0 and 4.0 MPa) were carried out to investigate the optimization, as shown in Figure 6. It is revealed that in the pressure range studied the dependence of$STY_{C_{5+}}$ on macropore diameter was similar with the trend mentioned above. Variation of total pressure from 1.0 to 4.0 MPa had a positive effect on $STY_{C_{5+}}$, which can be mainly attributed to two factors: the enhancement of reaction activity and the high mass transfer driving force at high total pressure. Although higher pressure resulted in lower gas phase effective diffusivity, due to the fact that gas phase molecular diffusivities vary inversely with pressure (see Figure 6S in Supporting Information), this adverse effect can be compensated by the higher concentration of reactants within the pores at higher total pressure. The improvement on $STY_{C_{5+}}$ was more significant at the pressure range of 1.0 to 3.0 MPa compared with that at the range of 3.0 to 4.0 MPa. This can be attributed to the FTS intrinsic kinetics and the inhibition of CO partial pressure on reaction rate [5]. For the meso-macroporous catalyst pellet with the mesopore and macropore size of 8 nm and 200 nm respectively, increasing total pressure from 1.0 to 4.0 MPa led to the optimal$STY_{C_{5+}}$ increasing from 1.019 to 1.639 g/mL_{cat}·h with the optimal porosity from 0.56 to 0.6, at the reaction temperature of 513 K, the H_2/CO mole ratio of 2.0 and the filling degree of 0.6.

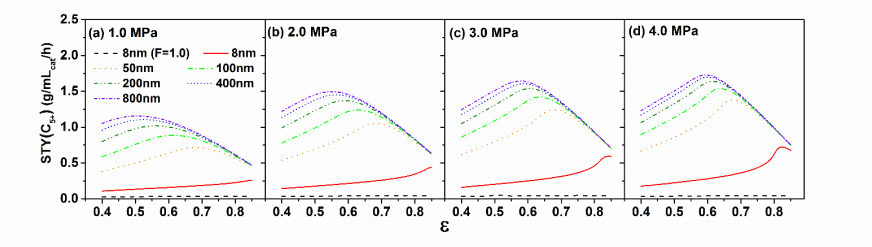

Figure 6 $STY_{C_{5+}}$ of the meso-macropores catalyst pellets with different macropore diameter at the total pressure of 1.0, 2.0, 3.0 and 4.0 MPa. The reaction temperature was 513 K, H_2/CO was 2.0, filling degree was 0.6, and other simulation parameters were adopted from Table 1.

5. CONCLUSIONS

A series of meso-macropore structured cobalt-loading catalyst with the same mesopore size (˜8 nm) and different macropore size (50-6000 nm) were prepared, characterized and evaluated. It was found that macropore diameter had remarkable influences on FTS activity and selectivity. The underlying reason was explored by a 1-dimensional steady state continuum model of the pellet. The simulation results found that the enhancement of mass transfer was primarily contributed by the decrease of filling degree and the increase of macroporosity with increasing macropore size, and less contributed by the reduction of Knudsen diffusion resistance.

The further simulation results of a 2 mm meso-macroporous pellet demonstrated that wax filling degree had a significant influence on mass transfer, and the optimal $STY_{C_{5+}}$ can be attained by increasing macropore size and adjusting porosity at different operation conditions. The enhancement on mass transfer by optimizing pore structure was more significant at high temperature. Besides, increasing pressure had a significant positive effect on $STY_{C_{5+}}$ from 1.0 to 3.0 MPa and then improved slightly with further increasing pressure to 4.0 MPa.

This work confirmed the mass transfer advantage of hierarchical structured cobalt-based catalyst pellets for FTS via elaborate adjustment of pore parameters, and thus the optimized hierarchical structured engineering pellets via simulation would be further validated and used in the industrial FTS. The research method presented in this work could be extended to pellet design for other gas-liquid-solid reactions.

ACKNOWLEDGMENTS

This work was financially supported by the Natural Science Foundation of China (Grant No. 21706271, 21736007, 21703273, 21902170, U1710104, and 21872162), the "Transformational Technologies for Clean Energy and Demonstration", Strategic Priority Research Program of the Chinese Academy of Sciences (Grant No. XDA 21020202), the Natural Science Foundation of Shanxi Province, China (Grant No. 201901D211582, 201801D221158, and 201903D121039), and the China Postdoctoral Science Foundation (Grant No. 2019M653488).

NOTATION

Roman

a	adsorption equilibrium constant (1/MPa)
c_i	concentration of component i (mol/m^3)
c^s_{CO}	concentration of CO at the external surface of the pellet (mol/m^3)
$\mathrm{d_p}$	pore diameter (nm)
$D_{\mathrm{e,i}}$	effective diffusivity of component i in catalyst pellet (m^2/s)
$D_{\mathrm{i,g}}$	gas phase comprehensive diffusivity of component i in pellet (m^2/s)
$D_{\mathrm{i,k}}$	Knudsen diffusivity of component i in pore (m^2/s)
$D_{\mathrm{i,m}}$	gas phase molecular diffusivity of component i in bulk (m^2/s)
$D_{\mathrm{i,j}}$	binary gas phase diffusivity (m^2/s)
f	kinetic correction factor
F	filling factor
k	reaction rate constant (mol/s·kg·MPa^2)
k_α	parameter for chain growth factor model
L	character diffusion length of the catalyst pellet (m)
$\mathrm{M_i}$	molecular weight of component i
P	total pressure (MPa)
$\mathrm{P_i}$	partial pressure for component i (MPa)
r	distance to the center of the pellet (mm)
r_p	pellet radius (mm)
R_p	pore radius (mm)
R	universal gas constant (J/mol·K)
R_{CO}	CO consumption rate (mol/kg$_{\mathrm{cat}}$·s)
$R_{\mathrm{co,total}}$	overall CO consumption rate per unit (mol/kg$_{\mathrm{cat}}$·s)
R^s_{CO}	CO consumption rate at the external surface of the pellet (mol/kg$_{\mathrm{cat}}$·s)
$\overline{R}_{\mathrm{CO}}$	dimensionless reaction rate of CO
Re	Reynolds number
Sc	Schmidt number
$S_{C_{5+}}$	selectivity of C_{5+} components (%)
$\mathrm{STY}_{C_{5+}}$	space-time yield f C_{5+} (g/mL$_{\mathrm{cat}}$·h)
T	temperature (K)
X	conversion (%)
x	dimensionless distance to the center of the pellet
y_i	mole fraction of component i

Greeks Letters

α	chain growth factor
α_{ave}	average chain growth factor
β	parameter for chain growth factor model
e	porosity
η	effectiveness factor
ρ_s	density of support skeleton (kg/m^3)
ρ_p	density of the catalyst pellet (kg/m3)
σ_{ij}	characteristic length, Å
υ_i	stoichiometric coefficient
Σ_v	diffusion volume
Φ	Thiele modulus
$\phi_i^{'}$	dimensionless Thiele modulus
Ψ_i	dimensionless concentration of component i

REFERENCES

1. Schulz H. Short history and present trends of Fischer-Tropsch synthesis. *Appl Catal, A.* 1999;186:3-12.

2. Martinelli M, Gnanamani MK, Demirel B, LeViness S, Jacobs G, Shafer WD. An Overview of Fischer Tropsch Process: Catalysts, Reactors and XtL Processes. *Appl Catal, A.* 2020.

3. Niu CC, Xia M, Chen CB, et al. Effect of process conditions on the product distribution of Fischer-Tropsch synthesis over an industrial cobalt-based catalyst using a fixed-bed reactor. *Appl Catal, A.* 2020;601:11.

4. Brunner KM, Perez HD, Peguin RPS, et al. Effects of Particle Size and Shape on the Performance of a Trickle Fixed-Bed Recycle Reactor for Fischer-Tropsch Synthesis. *Ind Eng Chem Res.*2015;54:2902-2909.

5. Mandić M, Todić B, Živanić L, Nikačević N, Bukur DB. Effects of Catalyst Activity, Particle Size and Shape, and Process Conditions on Catalyst Effectiveness and Methane Selectivity for Fischer–Tropsch Reaction: A Modeling Study. *Ind Eng Chem Res.* 2017;56:2733-2745.

6. Iglesia E, Soled SL, Baumgartner JE, Reyes SC. Synthesis and catalytic properties of eggshell cobalt catalysts for the Fischer-Tropsch Synthesis. *J Catal.* 1995;153:108-122.

7. Wang YN, Xu YY, Xiang HW, Li YW, Zhang BJ. Modeling of catalyst pellets for Fischer-Tropsch synthesis. *Ind Eng Chem Res.*2001;40:4324-4335.

8. Hubble R, York APE, Dennis JS. Modelling reaction and diffusion in a wax-filled hollow cylindrical pellet of Fischer Tropsch catalyst. *Chem Eng Sci.* 2019;207:958-969.

9. Post MFM, Vanthoog AC, Minderhoud JK, Sie ST. Diffusion Limitations in Fischer-Tropsch Catalysts. *AIChE J.*1989;35:1107-1114.

10. Froment GF, Bischoff KB, DeWilde J. Chemical Reactor Analysis and Design. 3rd ed. Hoboken, NJ: John Wiley & Sons, Inc; 2011.

11. Gardezi SA, Wolan JT, Joseph B. Effect of catalyst preparation conditions on the performance of eggshell cobalt/SiO_2 catalysts for Fischer-Tropsch synthesis.*Appl Catal, A.* 2012;447:151-163.

12. Fratalocchi L, Visconti CG, Lietti L, Tronconi E, Rossini S. Exploiting the effects of mass transfer to boost the performances of Co/γ-Al_2O_3 eggshell catalysts for the Fischer–Tropsch synthesis. *Appl Catal, A.* 2016;512:36-42.

13. Visconti CG, Tronconi E, Groppi G, et al. Monolithic catalysts with high thermal conductivity for the Fischer-Tropsch synthesis in tubular reactors. *Chem Eng J.* 2011;171:1294-1307.

14. Bukur DB, Mandic M, Todic B, Nikacevic N. Pore diffusion effects on catalyst effectiveness and selectivity of cobalt based Fischer-Tropsch catalyst. *Catal Today.* 2020;343:146-155.

15. Gheorghiu S, Coppens MO. Optimal bimodal pore networks for heterogeneous catalysis. *AIChE J.* 2004;50:812-820.

16. Dogu T. Diffusion and reaction in catalyst pellets with bidisperse pore size distribution. *Ind Eng Chem Res.*1998;37:2158-2171.

17. Johannessen E, Wang G, Coppens MO. Optimal distributor networks in porous catalyst pellets. I. Molecular diffusion. *Ind Eng Chem Res.* 2007;46:4245-4256.

18. Rao SM, Coppens MO. Mitigating Deactivation Effects through Rational Design of Hierarchically Structured Catalysts: Application to Hydrodemetalation. *Ind Eng Chem Res.* 2010;49:11087-11097.

19. Wang G, Coppens MO. Rational design of hierarchically structured porous catalysts for autothermal reforming of methane.*Chem Eng Sci.* 2010;65:2344-2351.

20. Wang G, Coppens MO. Calculation of the optimal macropore size in nanoporous catalysts and its application to DeNO(x) catalysis.*Ind Eng Chem Res.* 2008;47:3847-3855.

21. Wang G, Johannessen E, Kleijn CR, de Leeuwa SW, Coppens MO. Optimizing transport in nanostructured catalysts: A computational study.*Chem Eng Sci.* 2007;62:5110-5116.

22. Ye GH, Duan XZ, Sui ZJ, Zhu KK, Zhou XG, Yuan WK. Evaluation of approximations for concentration-dependent micropore diffusion in sorbent with bidisperse pore structure. *Adsorption.*2014;20:843-853.

23. Ye GH, Duan XZ, Zhu KK, Zhou XG, Coppens MO, Yuan WK. Optimizing spatial pore-size and porosity distributions of adsorbents for enhanced adsorption and desorption performance. *Chem Eng Sci.*2015;132:108-117.

24. Ye GH, Zhou XG, Yuan WK, Ye GH, Coppens MO. Probing pore blocking effects on multiphase reactions within porous catalyst particles using a discrete model. *AIChE J.* 2016;62:451-460.

25. Liu XL, Wang HL, Ye GH, Zhou XG, Keil FJ. Enhanced performance of catalyst pellets for methane dry reforming by engineering pore network structure. *Chem Eng J.* 2019;373:1389-1396.

26. Shi Y, Yang CF, Zhao XQ, et al. Engineering the Hierarchical Pore Structures and Geometries of Hydrodemetallization Catalyst Pellets. *Ind Eng Chem Res.* 2019;58:9829-9837.

27. Shi Y, Ye GH, Yang CF, et al. Pore engineering of hierarchically structured hydrodemetallization catalyst pellets in a fixed bed reactor. *Chem Eng Sci.* 2019;202:336-346.

28. Chen L, Zhang RY, Kang QJ, Tao WQ. Pore-scale study of pore-ionomer interfacial reactive transport processes in proton exchange membrane fuel cell catalyst layer. *Chem Eng J.* 2020;391.

29. Su J, Chai G, Wang L, et al. Pore-scale direct numerical simulation of particle transport in porous media. *Chem Eng Sci.*2019;199:613-627.

30. Liu SP, Cheng ZZ, Li Y, et al. Improved Catalytic Performance in Dimethyl Ether Carbonylation over Hierarchical Mordenite by Enhancing Mass Transfer. *Ind Eng Chem Res.*2020;59:13861-13869.

31. Li HS, Hou B, Wang JG, et al. Effect of hierarchical meso-macroporous structures on the catalytic performance of silica supported cobalt catalysts for Fischer-Tropsch synthesis. *Catal Sci Technol.* 2017;7:3812-3822.

32. Li HS, Wang JG, Chen CB, Jia LT, Hou B, Li DB. Effects of macropores on reducing internal diffusion limitations in Fischer-Tropsch synthesis using a hierarchical cobalt catalyst. *Rsc Adv.*2017;7:9436-9445.

33. Egaña A, Sanz O, Merino D, Moriones X, Montes M. Fischer–Tropsch Synthesis Intensification in Foam Structures. *Ind Eng Chem Res.* 2018;57:10187-10197.

34. Zhang XH, Su HQ, Yang XZ. Catalytic performance of a three-dimensionally ordered macroporous Co/ZrO2 catalyst in Fischer-Tropsch synthesis. *J Mol Catal A: Chem.* 2012;360:16-25.

35. Witoon T, Chareonpanich M, Limtrakul J. Effect of hierarchical meso-macroporous silica supports on Fischer-Tropsch synthesis using cobalt catalyst. *Fuel Process Technol.*2011;92:1498-1505.

36. Liu YF, Luo JJ, Girleanu M, Ersen O, Pham-Huu C, Meny C. Efficient hierarchically structured composites containing cobalt catalyst for clean synthetic fuel production from Fischer-Tropsch synthesis. *J Catal.* 2014;318:179-192.

37. Merino D, Pérez-Miqueo I, Sanz O, Montes M. On the Way to a More Open Porous Network of a Co–Re/Al_2O_3 Catalyst for Fischer–Tropsch Synthesis: Pore Size and Particle Size Effects on Its Performance. *Top Catal.* 2015;59:207-218.

38. Xu BL, Fan YN, Zhang Y, Tsubaki N. Pore diffusion simulation model of bimodal catalyst for Fischer-Tropsch synthesis.*AIChE J.* 2005;51:2068-2076.

39. Iglesia E. Design, synthesis, and use of cobalt-based Fischer-Tropsch synthesis catalysts. *Appl Catal, A.*1997;161:59-78.

40. Gardezi SA, Joseph B. Performance Characteristics of Eggshell Co/SiO_2 Fischer-Tropsch Catalysts: A Modeling Study. *Ind Eng Chem Res.* 2015;54:8080-8092.

41. Yates IC, Satterfield CN. Intrinsic Kinetics of the Fischer-Tropsch Synthesis on a Cobalt Catalyst. *Energy Fuels.*1991;5:168-173.

42. Vervloet D, Kapteijn F, Nijenhuis J, van Ommen JR. Fischer-Tropsch reaction-diffusion in a cobalt catalyst particle: aspects of activity and selectivity for a variable chain growth probability. *Catal Sci Technol.* 2012;2:1221-1233.

43. Pöhlmann F, Kern C, Rößler S, Jess A. Accumulation of liquid hydrocarbons in catalyst pores during cobalt-catalyzed Fischer–Tropsch synthesis. *Catal Sci Technol.* 2016;6:6593-6604.

44. Rößler S, Kern C, Jess A. Accumulation of liquid hydrocarbons during cobalt-catalyzed Fischer–Tropsch synthesis - influence of activity and chain growth probability. *Catal Sci Technol.* 2019;9:4047-4054.

45. Sánchez-López JRG, Martínez-Hernández A, Hernández-Ramírez A. Modeling of transport phenomena in fixed-bed reactors for the Fischer-Tropsch reaction: a brief literature review. *Rev Chem Eng.* 2017;33:109-142.

46. Marano JJ, Holder GD. Characterization of Fischer-Tropsch liquids for vapor-liquid equilibria calculations. *Fluid Phase Equilib.* 1997;138:1-21.

47. Erkey C, Rodden JB, Akgerman A. Diffusivities of Synthesis Gas and Normal-Alkanes in Fischer-Tropsch Wax. *Energy Fuels.*1990;4:275-276.

48. Erkey C, Rodden JB, Akgerman A. A Correlation for Predicting Diffusion-Coefficients in Alkanes. *Can J Chem Eng.*1990;68:661-665.

49. Rößler S, Kern C, Jess A. Sorption and condensation of higher hydrocarbons in a Fischer–Tropsch catalyst. *Catal Sci Technol.* 2019;9:1902-1910.

50. Pöhlmann F, Jess A. Interplay of reaction and pore diffusion during cobalt-catalyzed Fischer–Tropsch synthesis with CO2-rich syngas. *Catal Today.* 2016;275:172-182.

51. Wakao N, Smith JM. Diffusion in Catalyst Pellets.*Chem Eng Sci.* 1962;17:825-834.

52. Poling BE, Prausnitz JM, O'Connell JP. The Properties of Gases and Liquids. Fifth ed. New York: McGRAW-HILL; 2001.

53. Ertl G, Knozinger H, Schuth F, Weitkamp J. Handbook of Heterogeneous Catalysis. 2nd ed. Weinheim: Wiley 2008.

54. Liu ZT, Li YW, Zhou JL, Zhang BJ. Intrinsic Kinetics of Fischer-Tropsch Synthesis over an Fe-Cu-K Catalyst. *J Chem Soc Faraday Trans.* 1995;91:3255-3261.